Supplementary Information for

"Nitrogen-doped carbon coated $Li_3V_2(PO_4)_3$ derived from a facile *in-situ* fabrication strategy with ultrahigh-rate stable performance for lithium-ion storage" by

Cong Wang, Wei Shen, Haimei Liu*
State Key Laboratory of Chemical Resource Engineering, Beijing University of Chemical Technology, Beijing 100029, China

Further results and discussion:

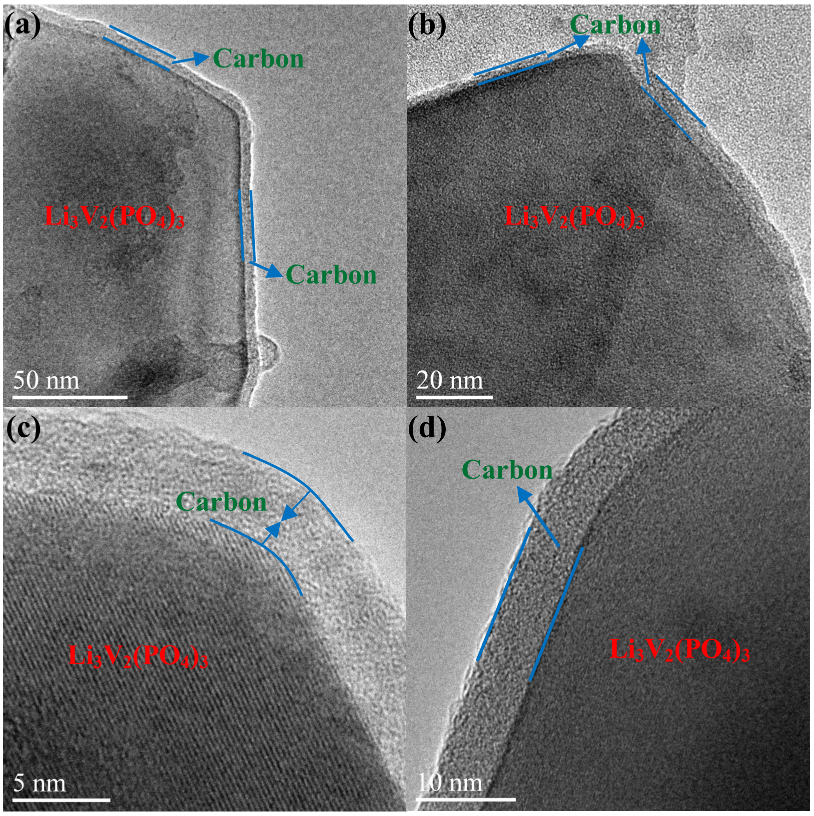

Fig. S1 TEM images of $Li_3V_2(PO_4)_3$/C+N materials.

Fig. S1 shows the TEM images of $Li_3V_2(PO_4)_3$/C+N materials, the $Li_3V_2(PO_4)_3$ particles are completely coated with an uniform nitrogen-carbon coating layer. It can be seen that the thickness of the nitrogen-doped carbon coating layer is about 5~10 nm. With the complete and uniform carbon coating, the electronic conductivity of $Li_3V_2(PO_4)_3$/C+N materials will be obviously improved, which will make positive effects on the electrochemical properties of $Li_3V_2(PO_4)_3$/C+N cathodes.

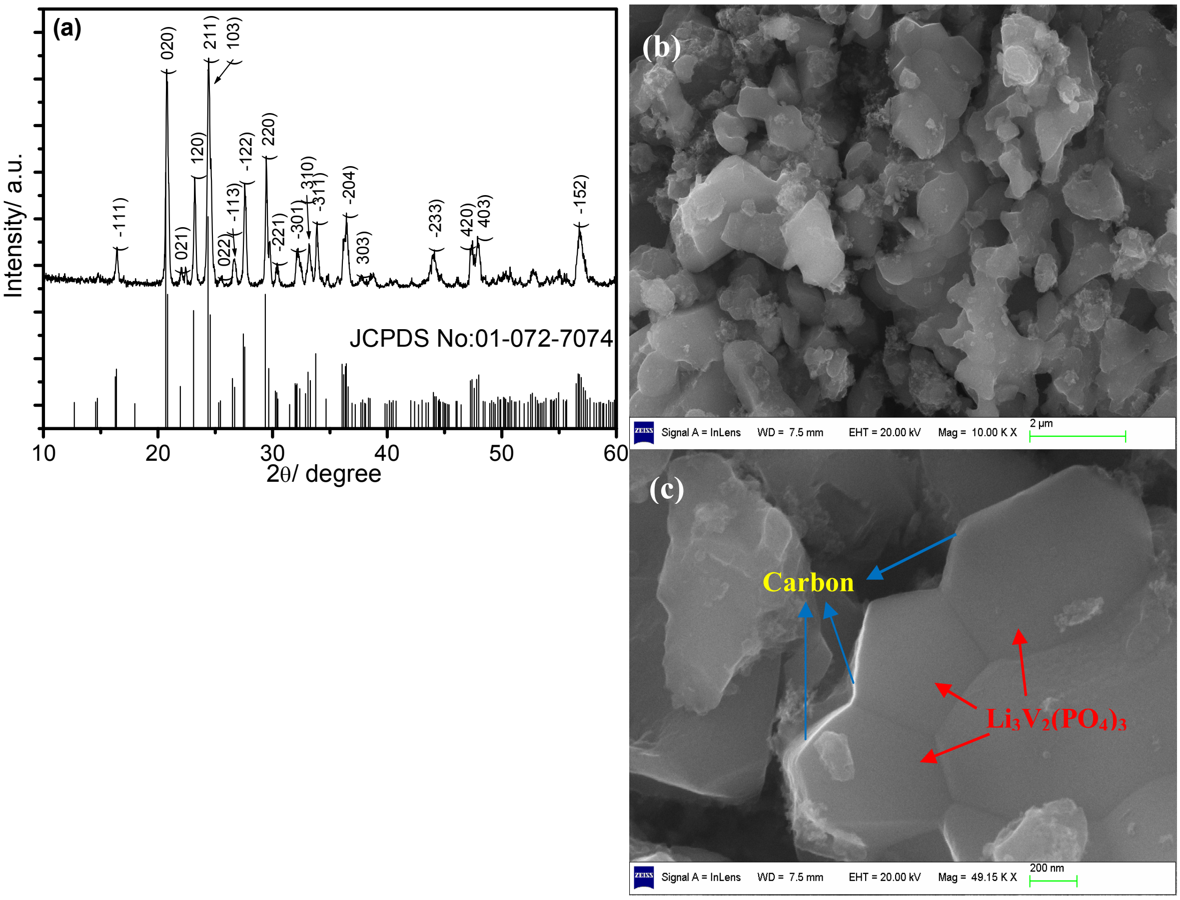

Fig. S2 Characterizations of the $Li_3V_2(PO_4)_3$/C+N materials; (a) XRD patterns; (b) and (c) SEM pictures.

The X-ray diffraction patterns of $Li_3V_2(PO_4)_3$/C+N composite are shown in **Fig. S2a.** It can be clearly seen that all the peaks correspond to a single phase of $Li_3V_2(PO_4)_3$ and can be indexed as a monoclinic structure with the space group $P2_1/n$. Based on the XRD analysis, there is no diffraction peaks from carbon, which indicates that the carbon coating layer is with an amorphous structure and/or the amount of the residual carbon layer on the surface of $Li_3V_2(PO_4)_3$/C+N composite is too little to be detected by the powder XRD.[S1] The SEM images, which are shown in **Fig. S2 b and c**, are used to analyze the morphology of $Li_3V_2(PO_4)_3$/C+N composite, it can be observed that the particle size of the $Li_3V_2(PO_4)_3$/C+N composite is about 1-2 µm and there is no obvious coalescence happens. As presented in **Fig. S2c**, the carbon coating layer can be clearly observed in the edge of the smaller $Li_3V_2(PO_4)_3$ particles.

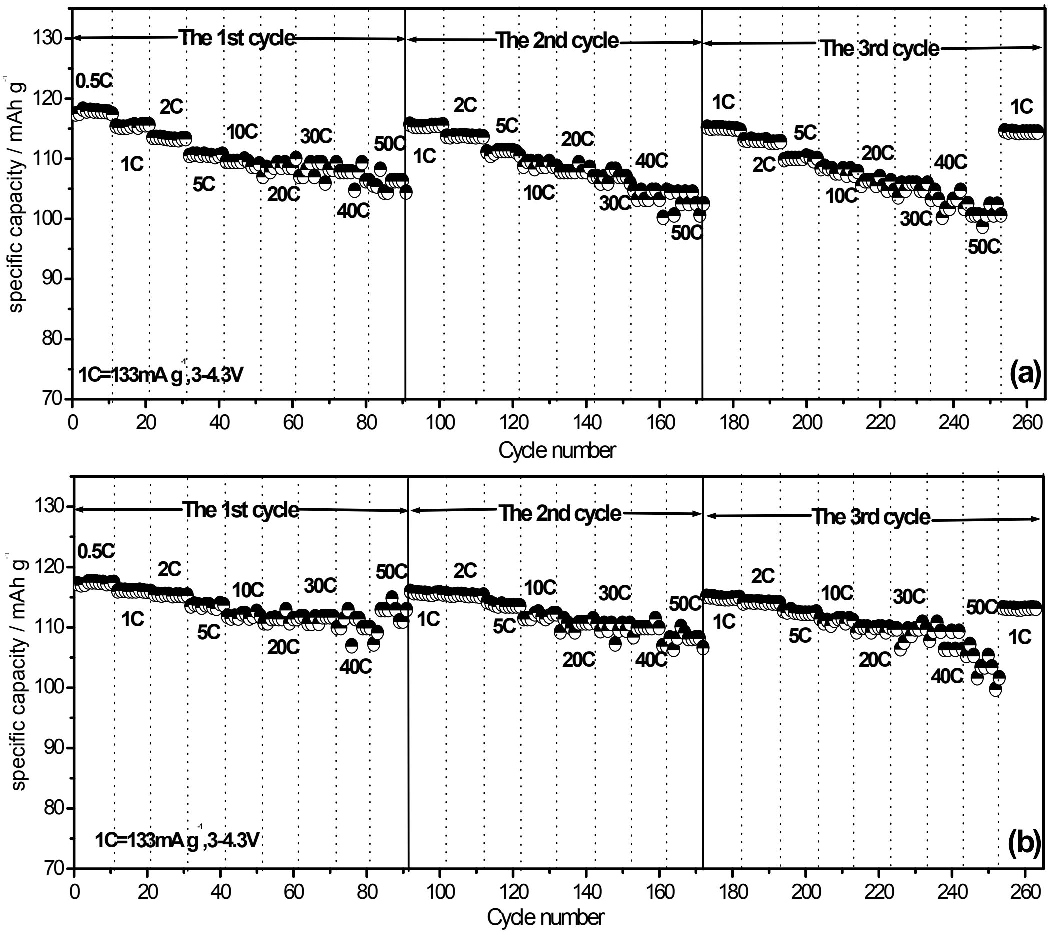

Fig. S3 The rate performances of the $Li_3V_2(PO_4)_3$/C+N materials under the charge current densities of (a) 5C and (b) 10C in the potential range of 3.0-4.3 V.

In order to confirm the impact of the charge current densities on the rate performance of $Li_3V_2(PO_4)_3$/C+N materials in the potential range of 3.0-4.3 V, the three times continuous overall rate capability tests from 0.5C to 50C (1C=133 mA g^{-1}) under the larger charge current densities of 5C and 10C are conducted and the results are shown in **Fig. S3**. It is obvious that, even under the larger charge current densities of 5C and 10C, the $Li_3V_2(PO_4)_3$/C+N composite still shows excellent ultrahigh-rate stable performance. When charged at 5C, even in the 1^{st} rate cycle, the 2^{nd} rate cycle and the 3^{rd} rate cycle discharged under 50C, which the discharge current densities increase from 1C to 50C in each rate cycle period, the capacity of $Li_3V_2(PO_4)_3$/C+N samples can still maintain at 105.8,103.3, 101 mAh g^{-1}, respectively. When re-cycled at 1C after three times continuous rate cycles, its discharge capacity can still reach 114.5 mAh g^{-1}. Similarly, when charged at 10C, even in the 1^{st} rate cycle, the 2^{nd} rate cycle and the 3^{rd} rate cycle period discharged under 50C, the capacity of $Li_3V_2(PO_4)_3$/C+N samples can still maintain at 111,108.1, 103.6 mAh g^{-1}, respectively. When re-cycled at 1C after three times continuous rate cycles, its discharge capacity can still reach 113.1 mAh g^{-1}. Both of which demonstrating the excellent rate performance of $Li_3V_2(PO_4)_3$/C+N cathode material.

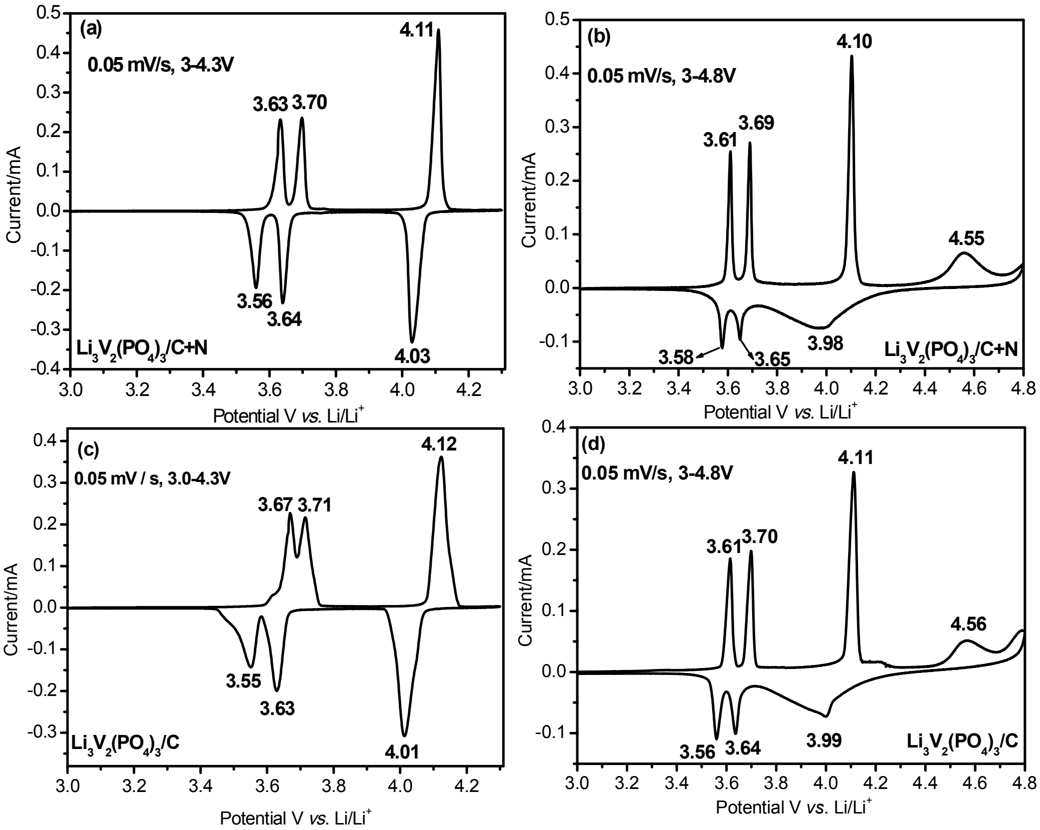

Fig. S4 Cyclic voltammogram curves of (a) and (b) $Li_3V_2(PO_4)_3$/C+N and (c) and (d) $Li_3V_2(PO_4)_3$/C samples at a scan rate of 0.05 mV s^{-1} in the potential range of 3-4.3 V and 3-4.8 V.

The CV (cyclic voltammogram) curves for the $Li_3V_2(PO_4)_3$/C+N and $Li_3V_2(PO_4)_3$/C in the potential ranges of 3.0-4.3 V and 3.0-4.8 V at a scan rate of 0.05 mVs^{-1} are presented in **Fig. S4.** Fig. S4a shows the CV curve for the $Li_3V_2(PO_4)_3$/C+N sample in the potential range of 3.0-4.3 V, there are three couples of anodic and the correspond cathodic peaks, located at 3.63, 3.70, 4.11 and 3.56, 3.64, 4.03 V, respectively. The first two anodic peaks correspond to the extraction of the first Li^+ with two steps, suggesting the formation of the $Li_{2.5}V_2(PO_4)_3$ and $Li_2V_2(PO_4)_3$,[S2] while the second Li^+ is removed via a single phase step corresponding to the third anodic peak of 4.11 V. The three cathodic peaks are attributed to reinsertion of the two Li^+ into the host lattice, accompanied with the V^{4+}/V^{3+} redox reaction. The CV curve for the $Li_3V_2(PO_4)_3$/C+N cathode in the potential range of 3.0-4.8 V is shown in Fig. S4b. There are four oxidation peaks located at 3.61, 3.69, 4.10 and 4.55 V, which corresponding to the phase transition from $Li_3V_2(PO_4)_3$ to $Li_xV_2(PO_4)_3$, where x=2.5, 2, 1 and 0, respectively, and three reduction peaks located at 3.58, 3.65 and 3.98 V, [S3] which corresponding to the reverse processes of the frontal three oxidation peaks in the curve. It is also illustrated that the extraction process of the third Li^+ in the $Li_3V_2(PO_4)_3$ is irreversible. It can be clearly observed in Fig. S4c and d that, whether in the potential range of 3.0-4.3 V or 3.0-4.8 V, the CV curves of $Li_3V_2(PO_4)_3$/C all have the similar shapes with that of $Li_3V_2(PO_4)_3$/C+N.

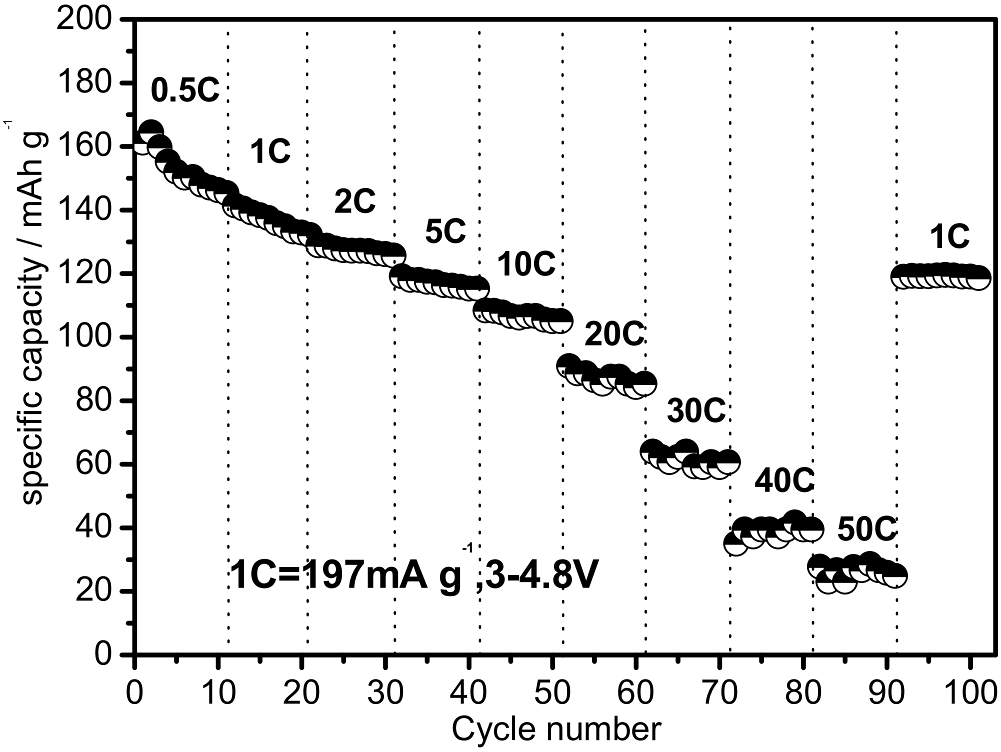

Fig. S5 The rate performance of the $Li_3V_2(PO_4)_3$/C+N materials in the potential range of 3.0-4.8 V.

The rate performance of the $Li_3V_2(PO_4)_3$/C+N materials in the potential range of 3.0-4.8 V is also be inspected and the results are shown in **Fig. S5**. When the $Li_3V_2(PO_4)_3$/C+N cathode is charged from 3.0 V to 4.8 V rather than 4.3 V, all three Li^+ in $Li_3V_2(PO_4)_3$ will be extracted and inserted. However, because of the extraction of the third Li^+ is the most kinetically hindered and an obvious electrochemical signature of solid solution behavior will be appeared when the potential upper limit increase to 4.8 V,[S3] both of which will constantly cause irreversible capacity in the cycling process. Therefore, as is observed in Fig. S5, during the rate cycling process in the potential of 3.0-4.8 V, it appears obvious capacity attenuation. When cycled at 0.5C (1C=197 mA g^{-1} in the potential of 3.0-4.8 V), the largest capacity of $Li_3V_2(PO_4)_3$/C+N in the potential range of 3.0-4.8 V can reach to 164.4 mAh g^{-1}, and even after cycling at 50C, its discharge capacity can still reach about 120 mAh g^{-1} when re-cycled at 1C, demonstrating a good rate performance, too.

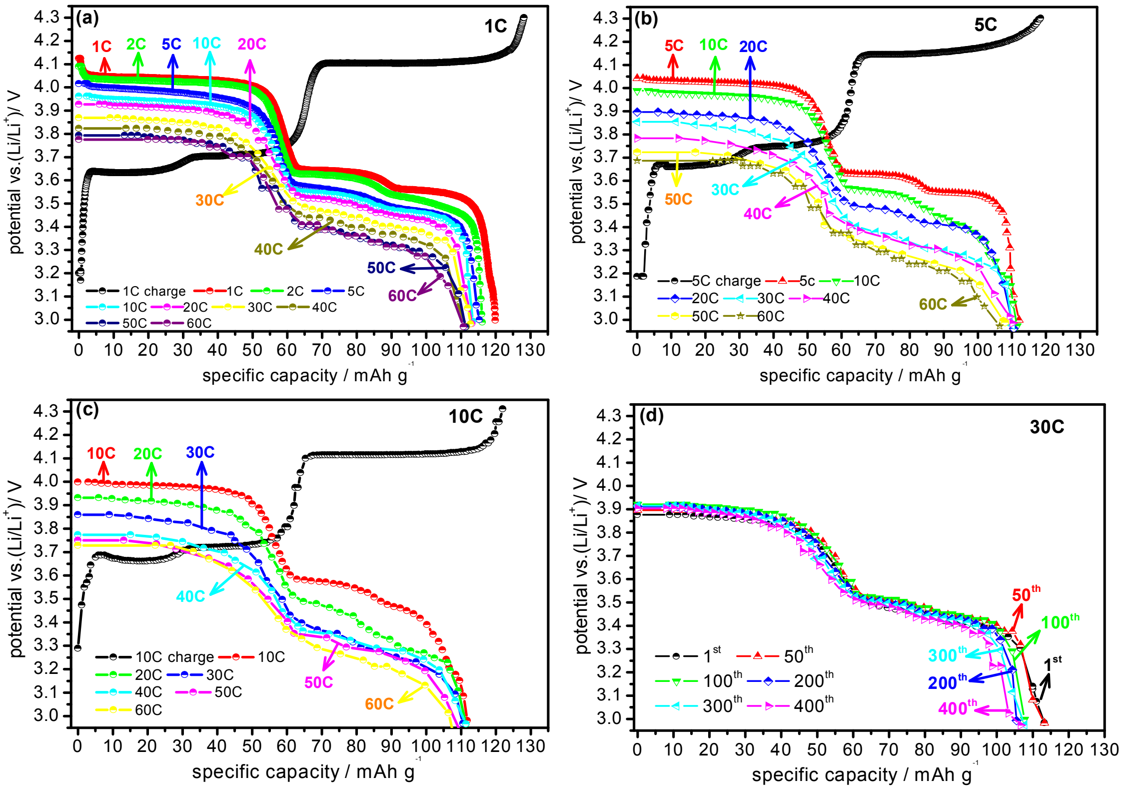

Fig. S6 The initial discharge curves of the $Li_3V_2(PO_4)_3$/C+N materials under various discharge current densities with different charge current densities of (a) 1C, (b) 5C and (c) 10C; (d) discharge curves of the $Li_3V_2(PO_4)_3$/C+N materials at various cycles under 30C; All the tests were worked in the potential window of 3.0- 4.3 V (vs. Li/Li^+).

Fig. S6a, b and c show the typical initial discharge curves of the $Li_3V_2(PO_4)_3$/C+N materials under various discharge current densities with different charge current densities of 1C, 5C and 10C between 3.0 and 4.3 V. Whether under any charge current densities, the initial specific capacities gradually decline and the plateaus in the curves gradually become unobvious with the increase of discharge current densities, which due to the electrochemical polarization becomes gradually aggravated along with the increase of the discharge current densities. For the discharge curve at 1C, three clear plateaus at 4.03, 3.64 and 3.56 V can be observed, which correspond to the transitions between the single phase $Li_xV_2(PO_4)_3$; x=2, 2.5 and 3.[S4] Fig. S6d shows the discharge curves at various cycles under a larger discharge current density of 30C, except a little decline of the specific capacity, there is nearly no obvious change in the discharge curves till 400 cycles. It is suggested that even under a quite large discharge current, the polarization on the electrode is not aggravated during the cycling process. All of the discharge curves in Fig. S6 indicate that the cycling performance of the $Li_3V_2(PO_4)_3$/C+N composite is excellent.

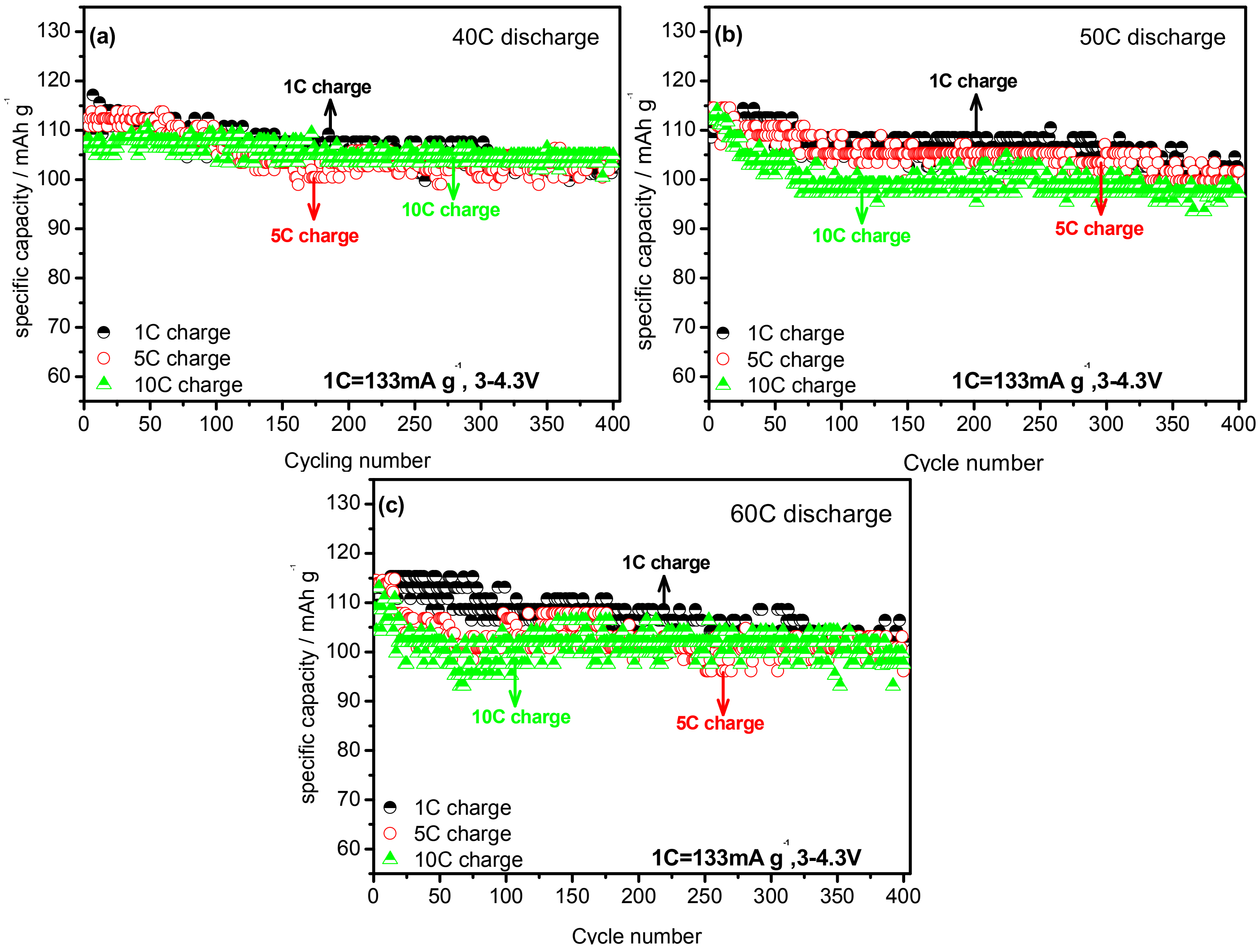

Fig. S7 The cycling properties of the $Li_3V_2(PO_4)_3$/C+N materials under the discharge current densities of (a) 40C, (b) 50C and (c) 60C with different charge current densities of 1C, 5C and 10C.

The cycle performances of $Li_3V_2(PO_4)_3$/C+N composite between 3.0 and 4.3 V discharged under 40C, 50C and 60C with different charge current densities of 1C, 5C and 10C are investigated and shown in **Fig. S7**. With the increase of the charge current densities, the specific capacity of $Li_3V_2(PO_4)_3$/C+N material appears a little attenuation, which due to the polarization becomes slightly aggravated. Even under the large charge current densities of 10C, the initial capacities of $Li_3V_2(PO_4)_3$/C+N under the discharge current capacities of 40C, 50C and 60C can attain to 107.9, 112 and 108.6 mAh g^{-1}, respectively; when cycled after 400 cycles, its specific capacities are still stabilized at 104.9, 97.3 and 97.5 mAh g^{-1}, respectively. So the effect of the charge current density on the long cycling stability of $Li_3V_2(PO_4)_3$/C+N materials under large discharge current density is not obvious. This $Li_3V_2(PO_4)_3$/C+N composite indeed shows the excellent cycling performance under large discharge current densities.

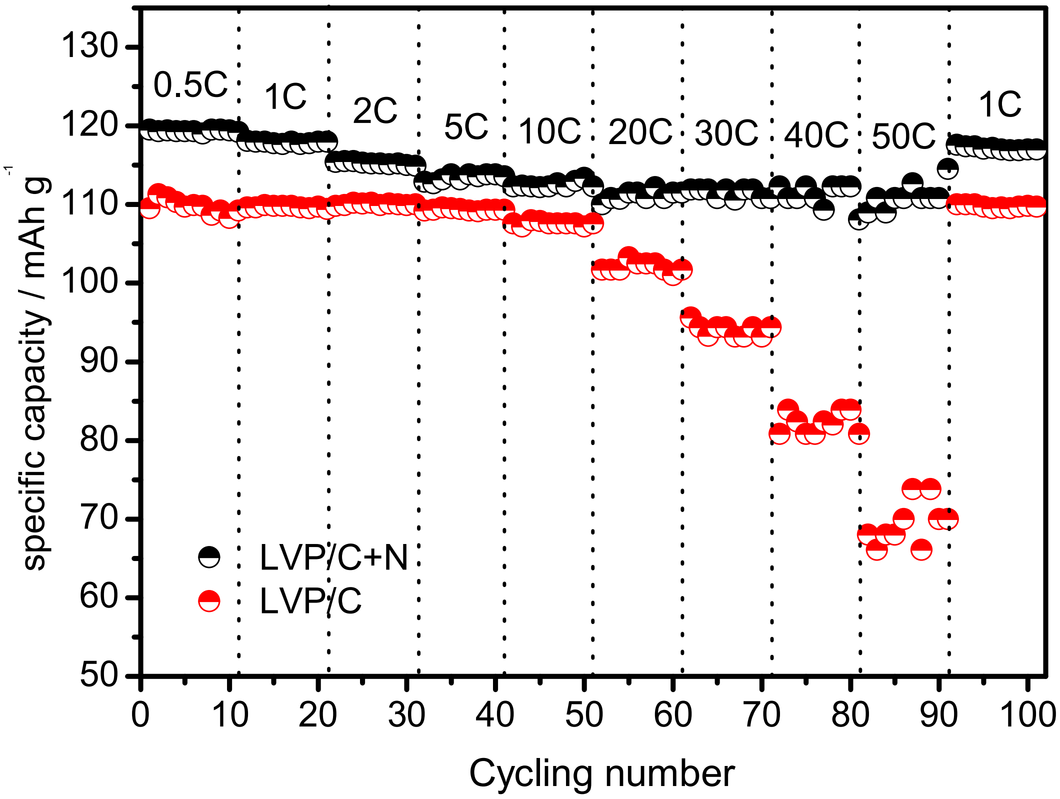

Fig. S8 A comparison of the rate capability between $Li_3V_2(PO_4)_3$/C+N (referred as LVP/C+N) and $Li_3V_2(PO_4)_3$/C (referred as LVP/C+N) sample. All the tests were worked in the potential window of 3.0 – 4.3 V (vs. Li/Li^+).

Fig.S8 presents the overall rate performances of $Li_3V_2(PO_4)_3$/C+N and $Li_3V_2(PO_4)_3$/C in the potential range of 3.0-4.3 V from 1C to 50C. The specific capacity of $Li_3V_2(PO_4)_3$/C+N sample ranges from 119.5 mAh g^{-1} at 1C to 110.8 mAh g^{-1} at 50C, and when re-cycled at 1C again, the specific capacity can still reach119.7 mAh g^{-1}. However, for $Li_3V_2(PO_4)_3$/C sample, its discharge capacity is sharply decreased to 69.6 mAh g^{-1} at 50C from 110.5 mAh g^{-1} at 1C. The rate performance of the $Li_3V_2(PO_4)_3$/C+N material is apparently superior to the $Li_3V_2(PO_4)_3$/C sample.

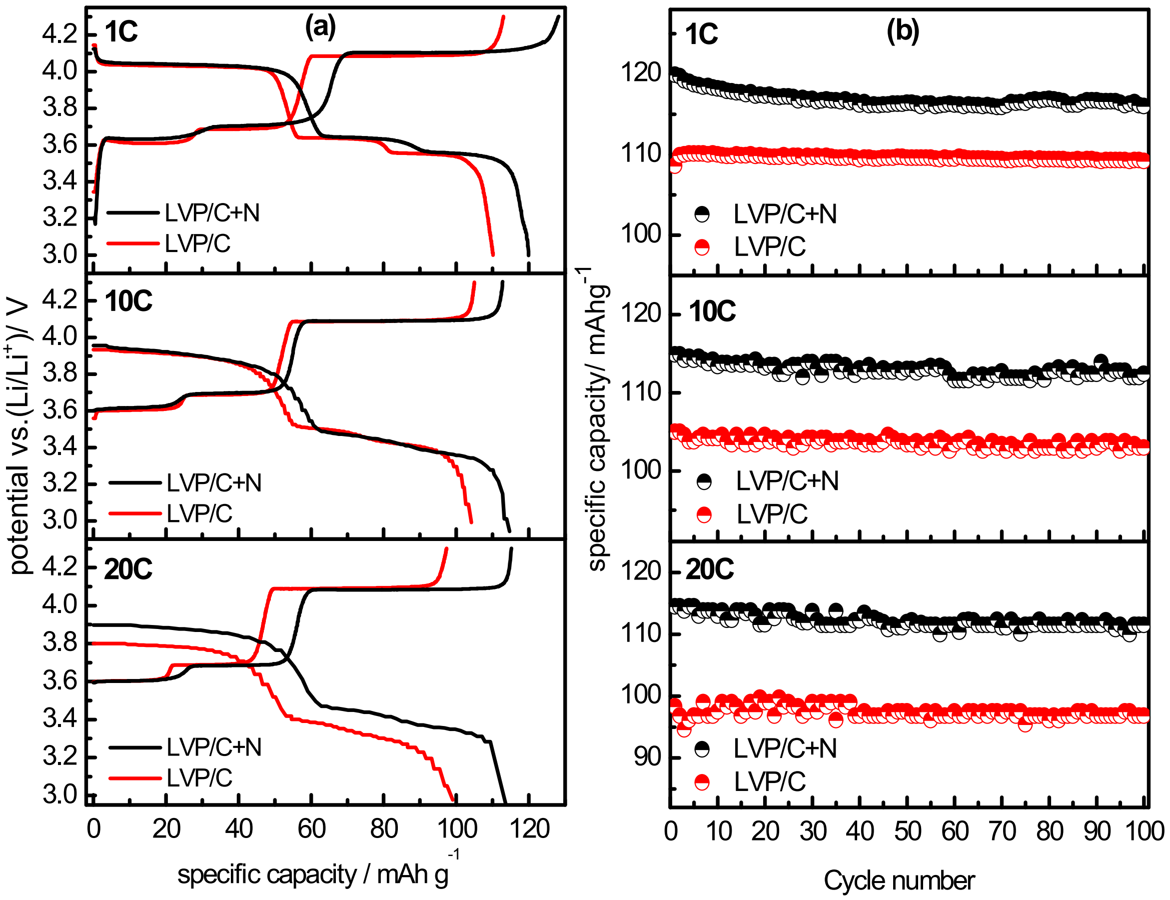

Fig. S9 (a) The initial charge-discharge curves and (b) cycle performances of the $Li_3V_2(PO_4)_3/C$ (referred as LVP/C) and $Li_3V_2(PO_4)_3/C+N$ (referred as LVP/C+N) samples at various current densities in the potential window of 3.0 – 4.3 V (vs. Li/Li^+).

Fig. S9a displays the initial charge-discharge curves of $Li_3V_2(PO_4)_3/C$ and $Li_3V_2(PO_4)_3/C+N$ at the current densities of 1C, 5C and 10C in the potential window of 3.0-4.3 V *vs*. Li/Li^+. Both the samples exhibit three discharge plateaus at about 4.10, 3.61 and 3.55 V at 1C, which corresponding to the insertion of lithium ions and the phase transition of $Li_XV_2(PO_4)_3$ from X=1.0 to 2.0, 2.5, 3.0, respectively. With the current densities increased to 10C and 20C, the platform in the profiles become unobvious. For $Li_3V_2(PO_4)_3/C+N$, an initial discharge capacity of 119.9, 115.1 and 114.1 mAh g^{-1} are obtained at 1C, 10C and 20C rate, respectively. As for $Li_3V_2(PO_4)_3/C$, its initial discharge capacity at 1C , 5C and 10C are 110.3, 103.5 and 99.7 mAh g^{-1}, respectively. The cycle performances of these two samples at different current densities are shown in Fig. **S9b**. It is noticed that at all current densities, the cycle stabilities of $Li_3V_2(PO_4)_3/C+N$ is better than that of $Li_3V_2(PO_4)_3/C$ and the specific capacities of the $Li_3V_2(PO_4)_3/C+N$ are obviously higher than that of $Li_3V_2(PO_4)_3/C$.

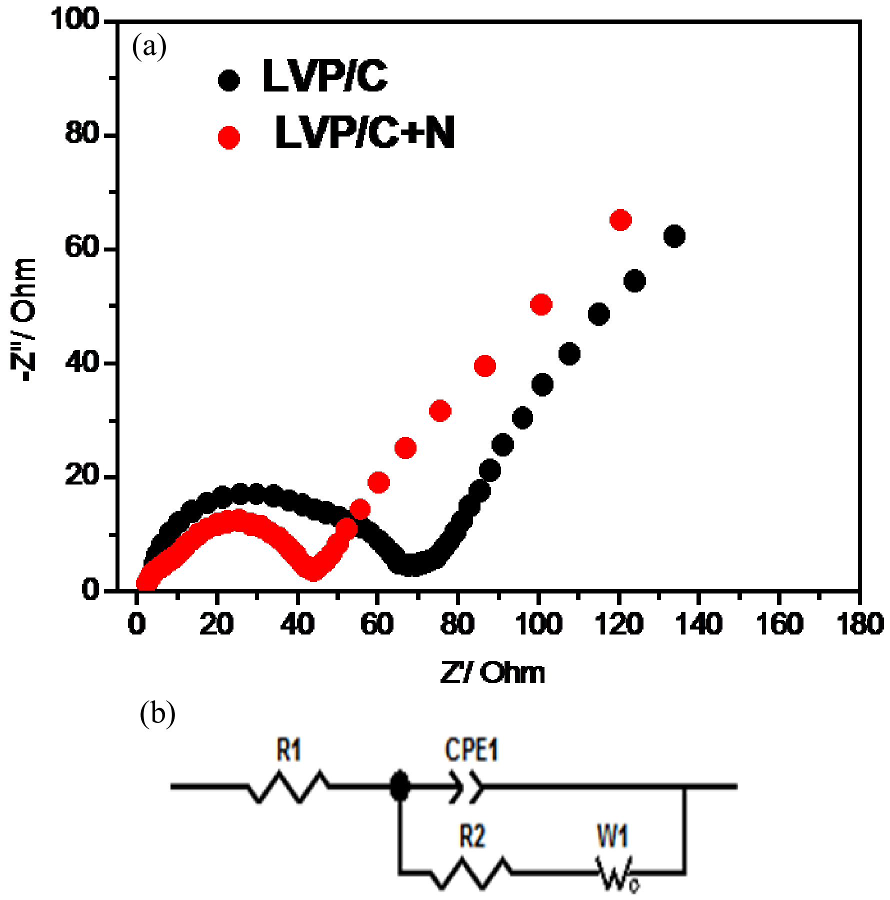

Fig. S10 (a) Nyquist plots for LVP/C ($Li_3V_2(PO_4)_3/C$) and LVP/C+N ($Li_3V_2(PO_4)_3/C+N$) composites at a stage of charge (4.3 V); (b) equivalent circuit used for simulating the experimental impedance data.

In order to further understand the electrochemical behaviors of the LVP/C ($Li_3V_2(PO_4)_3/C$) and LVP/C+N ($Li_3V_2(PO_4)_3/C+N$) samples, electrochemical impendence spectroscopy (EIS) measurements are carried out in the frequency range of 100 kHz to 10 mHz at the charge state (4.3 V) at the first cycle, and the Nyquist plots of the above two samples are shown in **Fig. S10a**. **Fig. S10b** presents an equivalent circuit to simulate the electrochemical impedance spectroscopy. R_1 represents the solution resistance; R_2 stands for the related charge-transfer resistance (R_{ct}); W_o represents the diffusion-controlled Warburg impendance in the low freqiency; CPE1 represents the double layer capacitance. It is found that the R_l (R_{ct}) value of LVP/C+N electrode (44.1 Ω) is smaller than that of LVP/C (68.6 Ω), indicating that the electron can transfer more quickly due to the N-doping in the carbon layer. Thus, the LVP/C+N ($Li_3V_2(PO_4)_3/C+N$) exhibits improved electronic conductivity and excellent electrochemical performance.

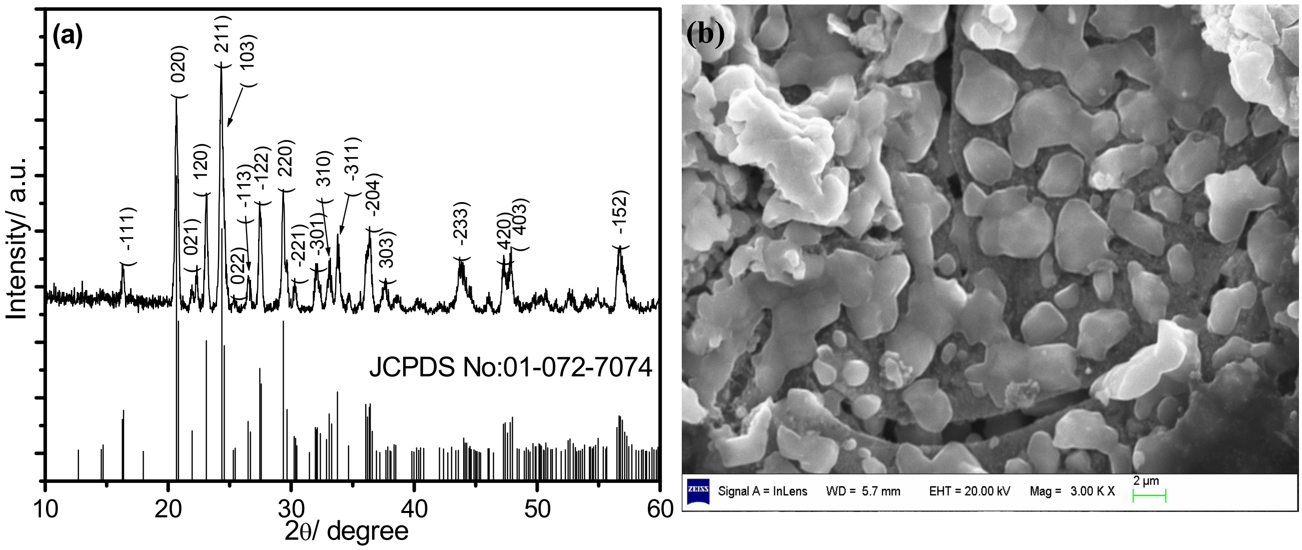

Fig. S11 Characterizations of the normal $Li_3V_2(PO_4)_3$/C+N materials, which was synthesized by an identical sol-gel method in the absence of freeze-drying process; (a) XRD patterns; (b) SEM picture.

For comparison, a sample of normal $Li_3V_2(PO_4)_3$/C+N composite was synthesized by an identical sol-gel method in the absence of freeze-drying process. The material characterizations and electrochemical performances of normal $Li_3V_2(PO_4)_3$ /C+N composite are shown in Fig. S11 to Fig. S15. The XRD patterns of the normal $Li_3V_2(PO_4)_3$ /C+N composite are shown in **Fig. S11a**. It can be clearly seen that all the peaks correspond to a single phase of $Li_3V_2(PO_4)_3$ and can be indexed as a monoclinic structure with the space group $P2_1/n$. **Fig. S11b** shows the morphology of normal $Li_3V_2(PO_4)_3$ /C+N composite. From the SEM observations, there are a lot of fine irregular particles with an average size of about 3~5 µm.

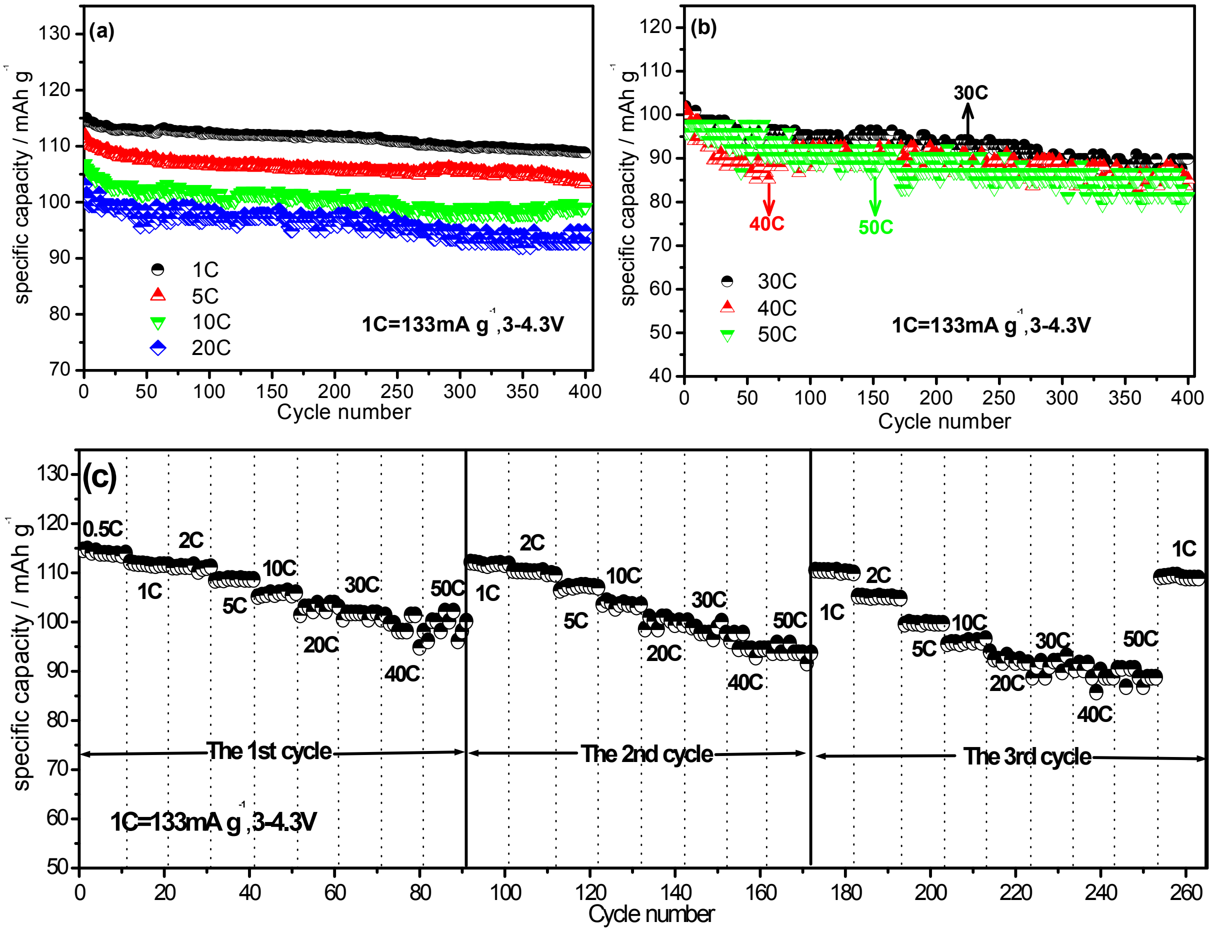

Fig. S12 The electrochemical properties of the normal $Li_3V_2(PO_4)_3$/C+N materials ,which was synthesized by an identical sol-gel method in the absence of freeze-drying process: (a) and (b) cycle performances at various current densities; (c) the rate performances; all the tests were worked in the potential window of 3.0- 4.3 V (vs. Li/Li^+).

The electrochemical properties of the normal $Li_3V_2(PO_4)_3$ /C+N composite in the potential range of 3.0-4.3 V are presented in **Fig. S12** and Fig. S13. **Fig. S12a** and **b** show the cycle performances of the normal $Li_3V_2(PO_4)_3$ /C+N composite under various current densities (from 1C to 50C). At 1C rate, its initial capacity is 115 mAh g^{-1}; when cycled to 400 cycles, its specific capacity still retains at 108.8 mAh g^{-1}, the capacity retention ratio is 94.6 %. Even at the higher current densities of 30C, 40C and 50C, its discharge capacity also exhibits perfect retention from an initial value of 102.1, 101.5 and 96 mAh g^{-1} and finally stabilized at 89.8, 85.6 and 81.6 mAh g^{-1} at 400 cycles, respectively. **Fig. S12c** presents a long rate cycle capability test of the normal $Li_3V_2(PO_4)_3$/C+N, even in the 1st rate cycle, the 2nd rate cycle and the 3rd rate cycle under 50C, which the discharge current densities increase from 1C to 50C in each rate cycle, the capacity of $Li_3V_2(PO_4)_3$/C+N samples can still maintain at 101, 94.3, 90.0 mAh g^{-1}, respectively. When re-cycled at 1C after three times continuous rate cycles, its discharge capacity can still reach 109.5 mAh g^{-1}. Although the electrochemical performances of the normal $Li_3V_2(PO_4)_3$/C+N composite, which was synthesized by an identical sol-gel method in the absence of freeze-drying process, is inferior to the $Li_3V_2(PO_4)_3$ /C+N composite which obtained from the freeze-drying process, it is still shows considerable long cycling life under large discharge current densities and good rate performance. The all above good electrochemical performances are ascribed to the uniform nitrogen-doped carbon coating: on one hand, obviously improves the electronic conductivity of the $Li_3V_2(PO_4)_3$ particles, on the other hand, supplies more defects and active sites in the carbon layers.

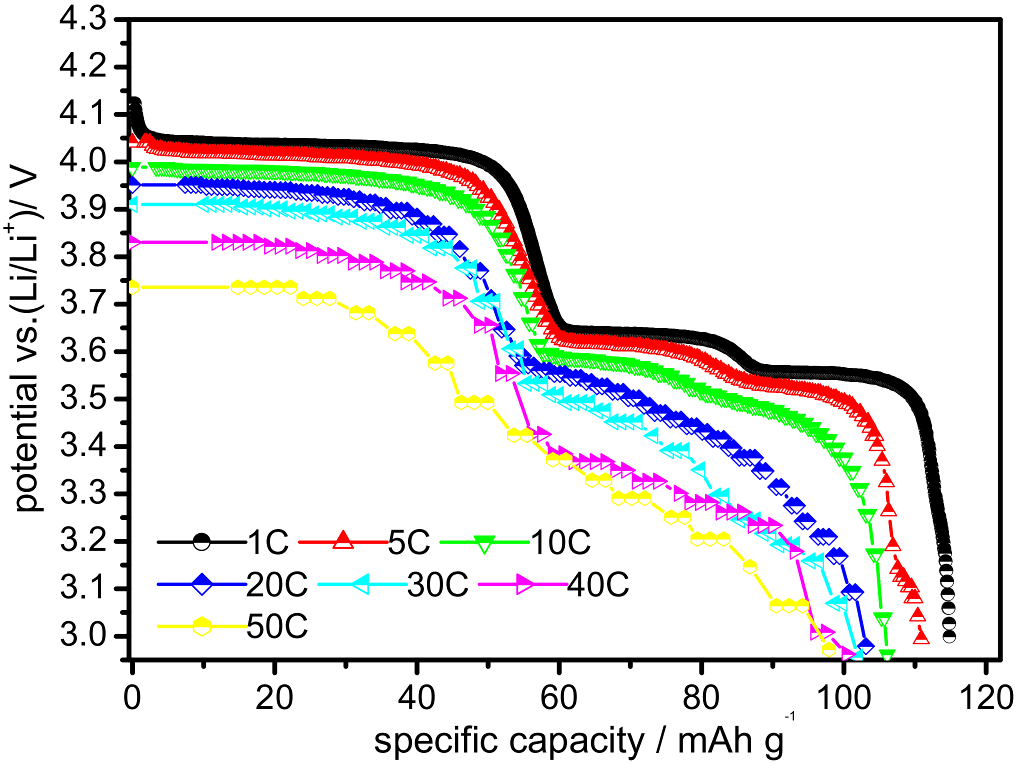

Fig. S13 The initial discharge curves of the normal $Li_3V_2(PO_4)_3$/C+N materials, which was synthesized by an identical sol-gel method in the absence of freeze-drying process, under various discharge current densities.

Fig. S13 shows the typical initial discharge curves of the normal $Li_3V_2(PO_4)_3$/C+N materials under various discharge current densities in the potential 3.0-4.3 V. With the increase of discharge current densities, the initial specific capacities gradually decline and the plateaus in the curves gradually become unobvious, which due to the electrochemical polarization becomes gradually aggravated along with the increase of the discharge current densities.

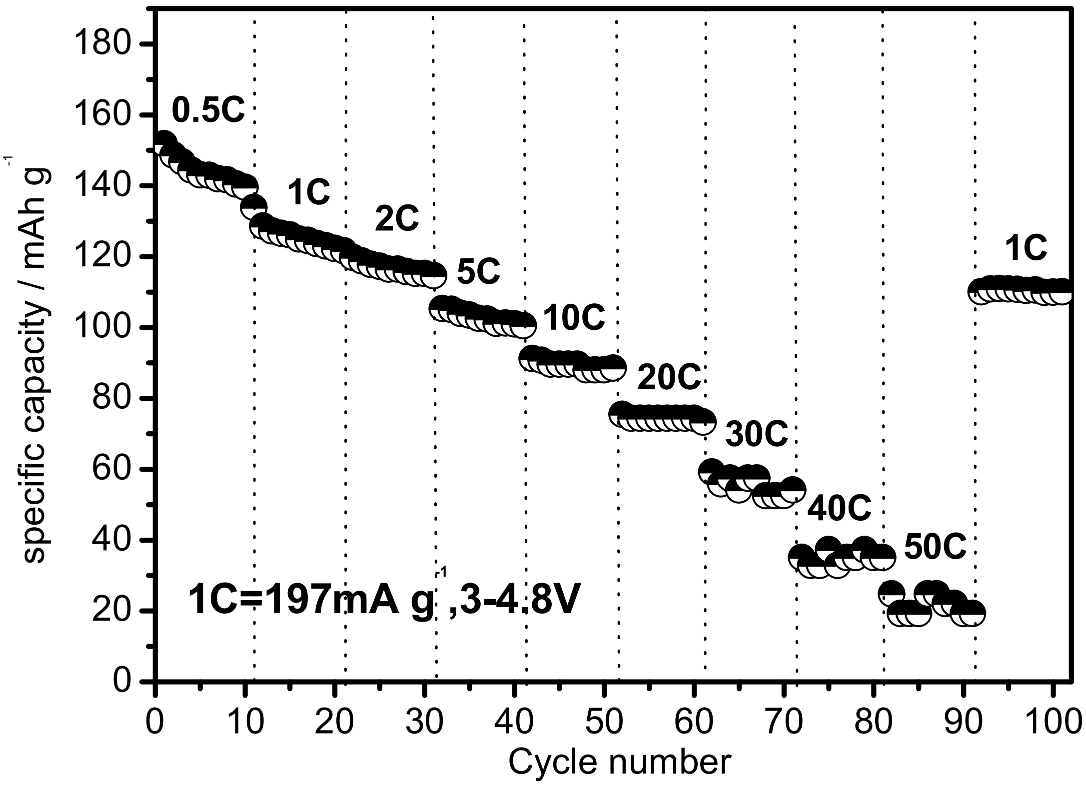

Fig. S14 The rate performance of the normal $Li_3V_2(PO_4)_3$/C+N materials which was synthesized by an identical sol-gel method in the absence of freeze-drying process in the potential range of 3.0-4.8 V.

Fig. S14 shows the rate performance of the normal $Li_3V_2(PO_4)_3$ /C+N composite in the potential range of 3.0-4.8 V. Because of the irreversibility for the extraction of the third Li^+ during the cycling process,[S3] with the increase of the discharge current densities and the cycling numbers, the capacity attenuation becomes more and more obvious. When cycled at 0.5C (1C=197 mA g^{-1} in the potential of 3.0-4.8 V), the largest capacity of the normal $Li_3V_2(PO_4)_3$/C+N in the potential range of 3.0-4.8 V can reach to 151.8 mAh g^{-1}, and even after cycling at 50C, its discharge capacity can still reach about 110 mAh g^{-1} when re-cycled at 1C, demonstrating a considerable rate performance, too.

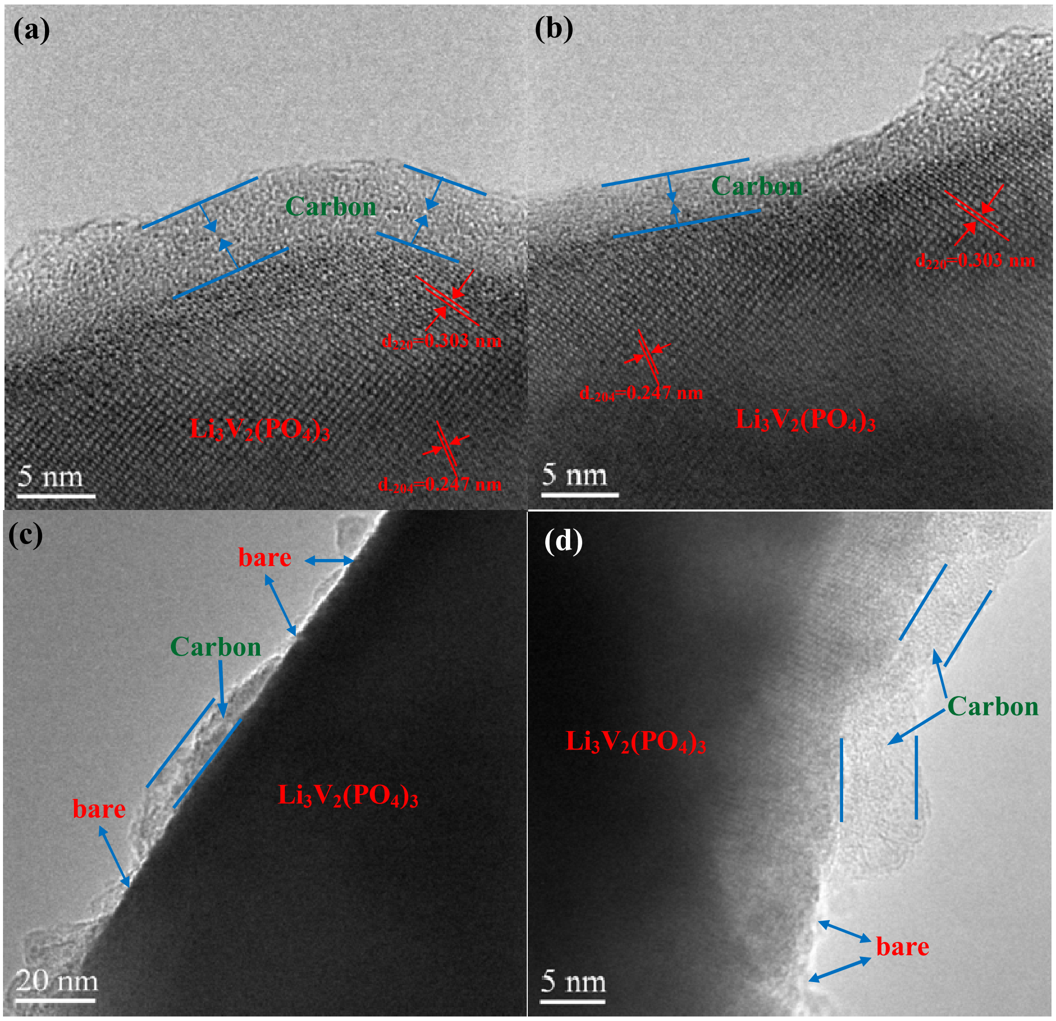

Fig. S15 The HRTEM images of the normal $Li_3V_2(PO_4)_3$/C+N materials which was synthesized by an identical sol-gel method in the absence of freeze-drying process.

The detailed features of the carbon-coating on the normal $Li_3V_2(PO_4)_3$/C+N materials which was synthesized in the absence of momentary freeze-drying process was explored by the HRTEM as depicted in **Fig. S15**. The HRTEM images in **Fig. S15 a and b** display clear lattice fringes with *d*-spacing of 0.247 nm and 0.303 nm, corresponding to the (-204) and (220) planes of the monoclinic $Li_3V_2(PO_4)_3$. There is a coated carbon layer with the thickness of 5-10 nm on the surface of the $Li_3V_2(PO_4)_3$ particles. However, as observed in **Fig. S15c and d,** compared with the momentary freeze-drying $Li_3V_2(PO_4)_3$/C+N (See in Fig. 1 and Fig. S1), the carbon layer on the $Li_3V_2(PO_4)_3$/C+N materials without freeze-drying process is quite inhomogeneous and incomplete and some areas are bare. The distinguish is due to the freeze-drying process, for the freeze-drying $Li_3V_2(PO_4)_3$/C+N, the microstructure of the precursor can be maintained and after sintered process a complete and uniform N-doped carbon coating layer can be achieved**.** As a result, after the use of freeze-drying process, the modification effects of the nitrogen-doped carbon coating can be further enhanced and the electrochemical performances of $Li_3V_2(PO_4)_3$/C+N material can be further improved.

References

S1 C. Wang, H. M. Liu and W. S. Yang, *J. Mater. Chem.*, 2012, **22**, 5281.

S2 S. C. Yin, P. S. Strobel, H. Grondey and L. F. Nazar, *Chem. Mater.* 2004, **16**, 1456.

S3 S. C. Yin, H. Grondey, P. Strobel, M. Anne and L. F. Nazar, *J. Am. Chem. Soc.*, 2003**, 125**, 10402.

S4 S. C. Yin, H. Grondey, P. Strobel, H. Huang and L. F. Nazar, *J. Am. Chem. Soc.*, 2003**, 125***,* 326.